Ab Initio Thermochemistry and Kinetics for Carbon-Centered Radical Addition and β-Scission Reactions

Maarten K. Sabbe,[‡] Aäron G. Vandeputte,[‡] Marie-Françoise Reyniers,*[,‡] Veronique Van Speybroeck,[†] Michel Waroquier,[†] and Guy B. Marin[‡]

Laboratorium voor Petrochemische Techniek, Ghent University, Krijgslaan 281 S5, B-9000 Gent, Belgium and Center for Molecular Modeling, Ghent University, Proeftuinstraat 86, B-9000 Gent, Belgium

Received: April 13, 2007; In Final Form: June 8, 2007

A quantitative comparison of ab initio calculated rate coefficients using five computational methods and five different approaches of treating hindered internal rotation and tunneling with experimental values of rate coefficients for nine carbon-centered radical additions/β scissions at 300, 600, and 1000 K is performed. The high-accuracy compound methods, CBS-QB3 and G3B3, and the density functionals, MPW1PW91, BB1K, and BMK, have been evaluated using the following approaches: (i) the harmonic oscillator approximation; (ii) the hindered internal rotor approximation for the internal rotation about the forming/breaking bond in the transition state and product; and the hindered internal rotation approximation combined with (iii) Wigner, (iv) Skodje and Truhlar, and (v) Eckart zero-curvature tunneling corrections. The density functional theory (DFT) based values for β-scission rate coefficients deviate significantly from the experimental ones at 300 K, and the DFT methods do not accurately predict the equilibrium coefficient. The hindered rotor approximation offers a significant improvement in the agreement with experimental rate coefficients as compared to the harmonic oscillator treatment, especially at higher temperatures. Tunneling correction factors are smaller than 1.40 at 300 K and 1.03 at 1000 K. For both the CBS-QB3 method, including the hindered rotor treatment but excluding tunneling corrections, and the G3B3 method, including hindered rotor and Eckart tunneling corrections, a mean factor of deviation with experimentally observed values of 3 is found.

1. Introduction

Hydrocarbon radical additions to unsaturated compounds and the reverse β-scissions contribute substantially to the product yields of many processes based on hydrocarbon radical chemistry. Among these processes are some of industry's largest scale production processes, such as steam cracking of hydrocarbons and polymerization. Radical additions are also important in processes based on oxidative chemistry, such as combustion, partial oxidation, or oxidative dehydrogenation. Optimizing the performance of these processes for a broad range of feedstocks and process conditions requires detailed and accurate kinetic models, often consisting of hundreds of species and thousands of elementary reactions.[1−3] For each elementary step in the reaction network, accurate thermodynamic and kinetic data are required. Sensitivity studies on these detailed kinetic models, such as the work of Zador et al. ,[4] point out that most of the uncertainty in the calculated product yields stems from inaccurate knowledge of kinetic and thermodynamic data. Moreover, if rate-based algorithms for network construction are applied,[5,6] then the availability of accurate rate data is even more important, because inaccurate kinetic data can result in the construction of an incomplete network that is not capable of grasping the chemistry underlying the process. Therefore, accurate thermodynamic and kinetic data for all reactions occurring in the reaction network are of crucial importance.

As the availability of experimental thermodynamic and kinetic data is by far insufficient to fulfill this need, a wide range of prediction methods, such as ab initio techniques or linear free energy relations, has been developed. Despite the enormous increase in computer performance during the past decades, it is still not feasible to calculate the required thermochemistry and rate coefficients using high-accuracy ab initio methods for all elementary reactions because reaction networks can contain up to thousands of reactions. Therefore, kinetic modeling relies on fast parametrized methods to predict kinetic parameters. These methods range from Evans−Polanyi relations[7,8] and thermochemical prediction methods[9] to methods relating the rate coefficients to the structure of the transition state.[10−15]

In this study we assess accurate, yet computationally feasible, ab initio methods to determine the thermochemistry and the rate coefficients for a set of nine addition reactions of carbon-centered hydrocarbon radicals to unsaturated hydrocarbons by comparing the rate coefficient predictions to experiment. Several computational methods for the calculation of electronic energies are evaluated including two high-level composite methods and three density functional theory (DFT) methods: the CBS-QB3 compound method of Montgomery et al.,[16] the G3B3 compound method of Baboul et al.,[17] the hybrid DFT functional MPW1PW91,[18] the DFT functional BB1K[19] optimized especially for kinetics, and the BMK[20] functional optimized as a tradeoff between thermodynamic and kinetic accuracy. Rate coefficients are determined within the conventional transition-state theory. The hindered rotor treatment of the internal rotation about the forming/breaking bond in the transition-state and in the product radical is compared with the harmonic oscillator approach for all modes. While the harmonic oscillator approximation provides a fast and straightforward method to determine the vibrational

* To whom correspondence should be addressed. Tel.: +32 9 264 5677; fax: +32 9 264 5824; e-mail: MarieFrancoise.Reyniers@ugent.be.
† Center for Molecular Modeling.
‡ Laboratorium voor Petrochemische Techniek.

10.1021/jp072897t CCC: $37.00
Published on Web 08/03/2007

frequencies corresponding to the internal modes, it breaks down for large-amplitude internal motions such as internal rotations. For addition reactions, the internal rotation about the forming bond in the transition-state has a low barrier corresponding to a low harmonic frequency. Hence, the harmonic oscillator vibrational partition function can be expected to diverge at higher temperatures, inducing significant inaccuracies on the calculated pre-exponential factor and/or activation energy. Moreover, this internal rotation is a transitional mode (i.e., a mode that is not present in the reactants), and hence, this mode directly influences the addition rate coefficient.[21] A correct description of this mode is therefore required. Heuts et al.[22] reported that the contribution to the pre-exponential factor made by the nontransitional modes is between 3 and 9 times smaller than the contribution made by the transitional modes. Therefore, the internal rotation about the forming bond is treated as a hindered internal rotation using the one-dimensional (1D) hindered rotor methodology of Van Speybroeck et al.[23−25] Next to that, three types of 1D zero-curvature tunneling corrections to the hindered rotor rate coefficients are considered (i.e., the methods of Wigner, Skodje and Truhlar, and Eckart). The rate coefficients obtained using the different computational approaches are compared to experimental rate coefficients. Kinetic parameters were fitted to the obtained rate data at $T = 300$, 600, and 1000 K by linear least-square regression to the Arrhenius equation.

2. Computational Procedures

The following set of hydrocarbon radical addition and reverse β-scission reactions was considered in this study:

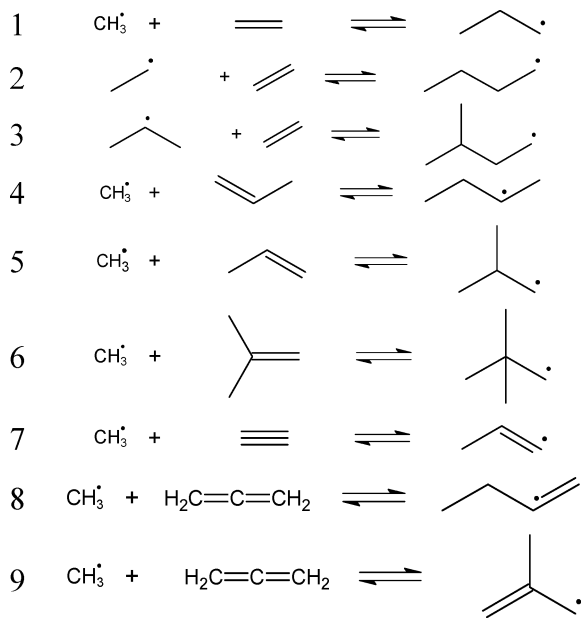

Calculated rate coefficients were compared with experimental values taken from the National Institute of Standards and Technology (NIST) chemical kinetics database.[26] The experimental values used in this study are tabulated at 300, 600, and 1000 K in Table 1. The set of available experimental rate coefficients consists of eight addition and six β-scission reactions. Values designated by NIST as "estimated, thermochemical, or other" or calculated values were excluded from the set of experimental data. Experimental values based on high and low-pressure extrapolations were rejected, except for the addition of ethyl to ethene (reaction 2) for which no other data at the selected temperatures were available.

2.1. Rate Coefficients. Rate coefficients are calculated based on conventional transition state theory in the high-pressure limit. For the bimolecular radical addition the rate coefficient is calculated according to eq 1:

$$k_{\infty}(T) = \kappa(T)\frac{k_B T}{h}\frac{n_{\mathrm{opt},\ddagger} q_{\ddagger}}{n_{\mathrm{opt,A}} q_A n_{\mathrm{opt,B}} q_B} e^{-\Delta E(0\ \mathrm{K})/RT} \quad (1)$$

the monomolecular β scission is calculated according to eq 2:

$$k_{\infty}(T) = \kappa(T)\frac{k_B T}{h}\frac{n_{\mathrm{opt},\ddagger} q_{\ddagger}}{n_{\mathrm{opt},P} q_P} e^{-\Delta E(0\ \mathrm{K})/RT} \quad (2)$$

where q is the total molar partition function per unit volume whereby the vibrational partition function is referred to the ground state vibrational level ("V=0" as used in the output of Gaussian 03[27] calculations), $\kappa(T)$ is the tunneling coefficient, and $\Delta E(0\ \mathrm{K})$ is the activation barrier at 0 K including zero-point vibrational energy (ZPVE). The number of optical isomers n_{opt} enters the equation because the partition functions are calculated for a single optical isomer whereas all configurations, including those that are not directly thermally accessible from the reference configuration, should be accounted for. External and internal symmetry numbers are contained within the partition functions.

Kinetic parameters were fitted to the obtained rate data at $T = 300$, 600, and 1000 K using linear least-square regression on the Arrhenius model;

$$\ln k = \ln A - \frac{E_a}{RT} \quad (3)$$

with k sampled at intervals of 50 K between $T = -100$ K and $T = +100$ K.

A comparison of the ab initio calculated rate coefficients to the experimentally observed values and discrimination between the different computational approaches were performed by averaging the ratios ρ, defined in eq 4.

$$\rho = \begin{cases} \dfrac{k_{\mathrm{calc}}}{k_{\mathrm{exp}}} & \text{for } k_{\mathrm{calc}} > k_{\mathrm{exp}} \\ \dfrac{k_{\mathrm{exp}}}{k_{\mathrm{calc}}} & \text{for } k_{\mathrm{exp}} > k_{\mathrm{calc}} \end{cases} \quad (4)$$

From this definition it follows that $\rho > 1$, so averaging the ρ ratios yields an indication of the overall deviation factor between calculated and experimental values. The factor ρ is calculated for every available experimental value. To prevent giving more weight to reactions with abundant experimental data, weighing factors are used to calculate the mean factor of deviation $\langle\rho\rangle$. The weighing factors account for the number of experiments $n_{\mathrm{exp},i}$ for reaction i (eq 5);

$$\langle\rho\rangle = \sum_{i}^{n_{\mathrm{reac}}} \frac{1}{n_{\mathrm{reac}}} \sum_{j}^{n_{\mathrm{exp},i}} \frac{1}{n_{\mathrm{exp},i}} \rho_{i,j} \quad (5)$$

where $\rho_{i,j}$ is equal to factor ρ of experiment j for reaction i and n_{reac} the total number of reactions. The mean factor of deviation $\langle\rho\rangle$ is used to identify the method yielding the best agreement to experimental values.

2.2. Transition State Geometry. The transition state geometries are obtained in the following way, using the Gaussian 03 package for all ab initio calculations.[27] First, the transition state is optimized at the B3LYP/6-311G(d,p) level using standard transition state search algorithms provided by Gaussian 03. From

TABLE 1: Experimental Rate Coefficients at 300, 600, and 1000 K from NIST[26a]

	k addition [m^3 $kmol^{-1}s^{-1}$]				k β-scission [s^{-1}]			
	ref	300 K	600 K	1000 K	ref	300 K	600 K	1000 K
1	Tsang 1986[c] Baulch 1992[c] Hogg 1964[d]	8.08×10^2 9.29×10^2 9.23×10^2	5.17×10^5 4.43×10^5	6.86×10^6	Bencsura 1992[b,c] Tsang 1988[c] Warnatz 1984[c] Mintz 1978[b]	6.88×10^{-10} 1.01×10^{-9}	6.45×10^1 1.10×10^2 2.38×10^2 3.54×10^2	1.54×10^6 2.86×10^6 1.65×10^7
2	Knyazev 1996[f]	5.49×10^2	2.67×10^5	5.60×10^6	Warnatz 1984[c] Kerr 1960[c,d]		1.32×10^3 1.53×10^3	2.00×10^7
3	Kerr 1959[d]	5.58×10^3						
4	Knyazev 1994[e] Tsang 1991[c] Baldwin 1987[b]	8.93×10^2 6.82×10^2	1.10×10^6 3.40×10^5 4.81×10^5	3.21×10^7 4.07×10^6	Tsang 1985[e] Warnatz 1984[c] Lin 1967[d]	4.89×10^{-9}	2.14×10^2 2.72×10^2 8.16×10^2	1.60×10^7
5	Tsang 1991[c] Baldwin 1987[b]	1.42×10^2	1.17×10^5 1.33×10^5	1.72×10^6	Tsang 1990[c] Warnatz 1984[c] Metcalfe 1960[d]	3.00×10^{-9}	2.45×10^2 1.86×10^3 1.89×10^3	5.68×10^6 1.26×10^7
6	Slagle 1991[e]		3.07×10^4		Tsang 1985[e] Szirovicza 1979[e] Szirovicza 1975[e]	2.06×10^{-9}	1.49×10^2 4.02×10^2 2.80×10^2	
7	Baulch 1992[c] Dominguez 1962[d]	1.36×10^3	9.07×10^5 3.94×10^5					
8	Scherzer 1983[d]		1.86×10^5					
9					Tsang 1973[e]			2.27×10^2

[a] Data type according to NIST chemical kinetics database: [b]experimental value, [c]literature review, [d]relative value normalized by reference value, [e]derived from fitting to a complex mechanism, [f]high or low-pressure extrapolation.

this geometry the $C-C_{B3LYP}$ bond length is extracted and is scaled using the correlation proposed by Saeys et al.[28] to bring the B3LYP/6-311G(d,p) transition state geometries in accordance with IRCMax (CBS-QB3; B3LYP/6-311G(d,p)) geometries.

$$C-C_{IRCMax} = 0.7381C-C_{B3LYP} + 58.03 \text{ pm} \quad \text{if } C-C_{B3LYP} > 225 \text{ pm}$$

$$C-C_{IRCMax} = C-C_{B3LYP} - 0.957 \text{ pm} \quad \text{if } C-C_{B3LYP} < 225 \text{ pm} \quad (6)$$

Finally, the transition state is reoptimized by constraining the length of the forming C−C bond at the $C-C_{IRCMax}$ bond length. The reoptimization is performed using the method for the subsequent energy calculation (i.e., B3LYP/6-311G(d,p) and B3LYP/6-31G(d) for the CBS-QB3 and G3B3 methods, respectively, and MPW1PW91, BB1K, and BMK for the other methods). The obtained geometry is applied for the calculation of the reaction barrier and the partition functions.

2.3. Reaction Barrier. The activation barrier at 0 K (ΔE(0 K)) is calculated using five different methods: (i) the CBS-QB3 complete basis set method of Montgomery et al.[16,29] This complete basis set method extrapolates the MP2 energy into a full basis set energy, after which higher-order contributions are added. This energy calculation is performed on a geometry optimized at the B3LYP/6-311G(d,p) level. The frequency analysis for the calculation of the ZPVE is done at the same level, using a scale factor of 0.99 for the harmonic frequencies; (ii) the G3B3 compound method, based on a complete basis set extrapolation of the UQCISD(T)/6-31G(d) on a B3LYP/6-31G(d) geometry. A scale factor of 0.96 on the harmonic frequencies is applied; (iii) the hybrid density functional MPW1PW91,[18] a non-dedicated general purpose density functional; (iv) the BB1K functional,[19] optimized for kinetics; and (v) the BMK functional,[20] optimized for an ideal tradeoff between kinetics and thermochemistry. All DFT based methods use the 6-311G(d,p) basis set. Because no scale factors are recommended these combinations of functionals and basis set, a harmonic frequency scaling factor of 0.99 is used, which is close to the value of 0.9877 advised by Andersson and Uvdal for scaling of DFT/triple-ζ ZPVEs.[30] The ΔE(0 K) reported in this study include ZPVE.

2.4. Partition Functions. Partition functions are evaluated using the standard procedure involving decoupling the translational, rotational, rovibrational, and electronic contributions, assuming a rigid external rotator and treating the internal modes within the harmonic oscillator approximation.

The hindered rotor partition function for the internal rotation about the forming bond in the transition state and the breaking bond in the product radical is calculated using the one-dimensional hindered rotor procedure (1D-HR) described by Van Speybroeck et al.[21] In this work, we adopt the notation "HR" for the application of this 1D uncoupled hindered internal rotor approach (1D-HR) to the internal rotation about the forming bond in the transition state and the formed bond in the product radical.

It has been shown that a fortuitous cancellation of errors makes the uncoupled 1D-HR scheme as successful as the fully coupled scheme.[23] A validation of this 1D-HR scheme is given in the work of Vansteenkiste et al.[25] In this 1D-HR procedure, the expressions for the reduced moment of inertia (I_{red}) for the rotation of two rigid tops relative to each other are equivalent to the so-called $I^{3,4}$ estimator of the moment of inertia as used by East and Radom.[31] This provides the exact I_{red} for a molecule with one rigid internal rotation. The potential energy profile for internal rotation ($V(\varphi)$) is approximated as a Fourier expansion (eq 7);

$$V(\varphi) = \sum_i^n \frac{V_i}{2}(1 - \cos i\varphi) + \sum_i^n V_i' \sin i\varphi \quad (7)$$

where $n = 3$, except for 6-fold symmetric rotors for which $n = 6$ is used. The coefficients V_i and V_i' are determined by fitting them to a B3LYP/6-31G(d) relaxed scan at 10° intervals of the

potential energy surface (PES) for internal rotation. The optimum is relocated at every step of the internal rotation to permit stretching of the forming C−C bond, which has an influence on the rotational barrier. Finally, the partition function is calculated by direct summation over the energy levels resulting from the Schrödinger equation for internal rotation.

The obtained hindered rotor partition function should replace the corresponding HO-vibrational partition function for this internal rotation. The internal vibrational modes provided by a harmonic frequency analysis are composed of several internal rotations, and it has been shown that replacing a vibrational partition function based on these harmonic frequencies yields unphysical results.[32] Hence, the procedure was not to replace one of these modes but to replace a vibrational partition function based on the frequency derived from the energy profile for internal rotation. This procedure assures a consistent 1D approach of the hindered rotation, in which a 1D vibrational partition function is replaced by a 1D internal rotation partition function.[25,32,33]

Adjusting the partition functions affects not only the rate coefficients but also derived quantities such as the Arrhenius parameters. For addition reactions, the influence of the HR treatment on the HO-activation energy can be evaluated from eq 8.

$$\begin{aligned} E_{a,HR} - E_{a,HO} &= RT^2\left(\frac{\partial}{\partial T}\ln\frac{k_{HR}}{k_{HO}}\right) \\ &= RT^2\left(\frac{\partial}{\partial T}\ln\frac{q_{HR}}{q_{HO}}\right) \\ &= RT^2\left(\frac{\partial}{\partial T}\ln\frac{q_{HR}^{int.rot.}}{q_{HO}^{int.rot.}}\right) \end{aligned} \quad (8)$$

For addition reactions, only the transition state partition function is modified, and the ratio between k_{HR} and k_{HO} can be simplified to the ratio of the transition state partition functions q_{HR} and $q_{HO.}$ This ratio (q_{HR}/q_{HO}) can be evaluated by the ratio of the partition functions of the internal rotation about the forming bond in the transition state in the hindered rotor and the harmonic oscillator descriptions, $q_{HR}^{int.rot.}$ and $q_{HO}^{int.rot.}$. For the pre-exponential factor A, the influence of the hindered rotor treatment is related to the change in the activation entropy $\Delta^{\ddagger}S$ (eq 9);

$$\begin{aligned} \ln A_{HR} - \ln A_{HO} &= (\Delta^{\ddagger}S_{HR} - \Delta^{\ddagger}S_{HO})/R \\ &= (S_{HR}^{int.rot.} - S_{HO}^{int.rot.})/R \\ &= \ln\frac{q_{HR}^{int.rot.}}{q_{HO}^{int.rot.}} + T\frac{\partial}{\partial T}\ln\frac{q_{HR}^{int.rot.}}{q_{HO}^{int.rot.}} \end{aligned} \quad (9)$$

where the superscript "int.rot." stands for the considered internal rotation in the transition state. If we assume generic rotational potential energy profiles, the effect of the barrier heights on the Arrhenius parameters can be evaluated in a straightforward way. This simplified picture provides an indication of the order of magnitude of the changes on the Arrhenius parameters that may be expected by taking into account the HR approach. Typical potential profiles for a methyl rotor (V_1) and an ethyl rotor (V_2), occurring in the transition state of a methyl and ethyl radical addition, respectively, to ethene are given by eq 10.

$$V_1(\varphi) = \frac{V_{max}}{2}(1 - \cos 3\varphi)$$

$$V_2(\varphi) = \frac{V_{max}}{2}\left(\frac{1 - \cos\varphi}{2} + \frac{1 - \cos 3\varphi}{2}\right) \quad (10)$$

Plots of q_{HR}/q_{HO} for V_{max} in the range of $0 - 60$ kJ mol^{-1}are shown in Figure 1 for both model energy profiles, as well as the effect of the HR approach on the pre-exponential factor and the activation energy. The calculations assumed a temperature of 1000 K and a reduced moment of inertia of 20 amu a_0^2 (9.37×10^{-47} kg m^2). Obviously, the difference between the HR and the HO treatment is large for barriers below 2 kJ mol^{-1} (q_{HR}/q_{HO} approaches zero). In the absence of higher energy conformers, as is the case for the model potential V_1, the effects on the rate coefficients and the Arrhenius parameters are significant for barriers to internal rotation smaller than 5−10 kJ mol^{-1} only. However, the presence of higher energy conformers, as is the case for potential V_2, increases the partition function, the activation energy, and the pre-exponential factor significantly, up to barriers of 60 kJ mol^{-1}. For the model potential energy profile V_2, the influence is most pronounced for a barrier of 40 kJ/mol, and the increase in activation energy amounts to 5 kJ mol^{-1}, whereas the pre-exponential factor A increases with a factor 3 ($\Delta\log A \cong 0.5$). At 1000 K, the HR treatment thus results in an increase of the rate coefficient with a factor of 1.7.

Comparing the free rotor (FR) and the hindered rotor approach for the same model potential energy profiles V_1 and V_2, it is found that at 1000 K the FR approximation is valid for rotational barriers below 2 kJ mol^{-1}, for which the FR and HR partition function differ by less than 10%. For rotational barriers larger than 10 kJ mol^{-1}, the difference between the FR and the HD approach exceeds a factor 2. At temperatures lower than 1000 K, the deviations between HR and FR increase rapidly with decreasing temperature. At 300 K, the FR partition function is within 10% of the HR partition function for rotational barriers lower than 0.5 kJ mol^{-1} only.

2.5. Thermochemistry. The HO reaction enthalpies and entropies are calculated in the standard HO approximation provided by Gaussian 03, using the scale factors reported above. The HR corrections to the HO values for the internal rotation about the formed bond in the product radical are determined using the standard expressions for enthalpy and entropy as a function of the partition functions taken from McQuarrie.[34] The hindered rotation correction on the partition function is calculated according to the procedure described above. The concentration-based equilibrium coefficient K_c is calculated by eq 11;

$$K_c = \frac{RT}{p}\,e^{-\Delta_r G^{\circ}/RT} \quad (11)$$

where $\Delta_r G^{\circ}$ is the standard reaction Gibbs free energy of reaction.

2.6. Tunneling Corrections. Quantum tunneling along the reaction coordinate is taken into account by three different 1D methods (i.e., the methods of Wigner,[35] Skodje and Truhlar[36] and Eckart[37]). The Wigner method, the most widely used approximation to account for tunneling through the reaction barrier, assumes a parabolic potential for nuclear motion near the transition state (eq 12).

$$\kappa(T) = 1 + \frac{1}{24}\left(\frac{h\,\mathrm{Im}(\nu^{\ddagger})}{k_B T}\right)^2 \quad (12)$$

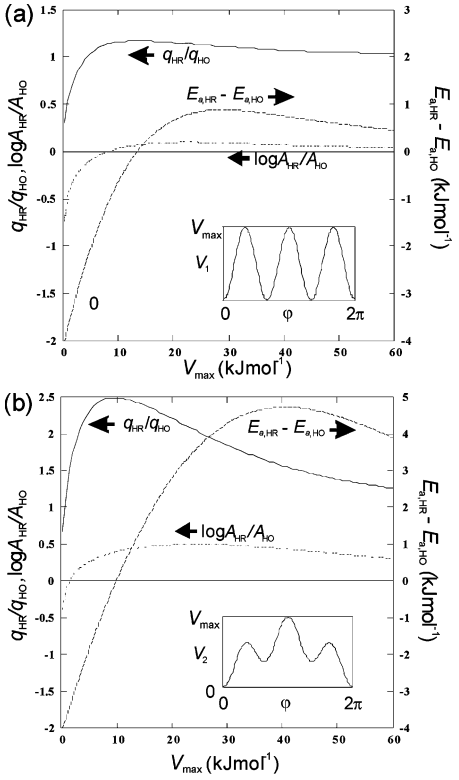

Figure 1. Influence on q, E_a, and log A of the hindered internal rotor treatment of the internal rotation about the forming bond in the transition state for two model potential energy profiles for internal rotation (I_{red} = 20 amu bohr^2, T = 1000 K, σ = 3 and 1, respectively).

This approximation holds for $k_bT \gg h\ \mathrm{Im}(\nu^{\ddagger})$. For radical addition reactions with a typical imaginary wavenumber of 500 cm^{-1}, this approximation is only valid for temperatures higher than 1000 K.

The method of Skodje and Truhlar depends not only on the curvature of the minimum energy path near the transition state but also on the height of the potential energy barrier. This method can be written in the following form;

$$\beta \le \alpha : \kappa(T) = \frac{\beta\pi/\alpha}{\sin(\beta\pi/\alpha)} - \frac{\beta}{\alpha - \beta} e^{[(\beta-\alpha)(\Delta V^{\ddagger}-V)]}$$

$$\alpha \le \beta : \kappa(T) = \frac{\beta}{\beta - \alpha}(e^{[(\beta-\alpha)(\Delta V^{\ddagger}-V)]} - 1) \qquad (13)$$

where $\alpha = (2\pi)/[h\ \mathrm{Im}(\nu^{\ddagger})]$ and $\beta = (k_BT)^{-1}$.[38]

The Eckart method accounts for the barrier height by fitting an Eckart potential to the stationary points so that it passes through the zero-point-corrected energies of the reactants, saddle point, and products (eq 14).

$$V(s) = \frac{a\, e^{\alpha(s-s_0)}}{1 + e^{\alpha(s-s_0)}} + \frac{b\, e^{\alpha(s-s_0)}}{(1 + e^{\alpha(s-s_0)})^2} + c \qquad (14)$$

Using this potential, the Schrödinger equation accounting for tunneling can be solved exactly, allowing the construction of an analytical form of the transmission probability. To determine the quantum tunneling coefficient, the expressions from Coote et al. were adopted.[39] The final integration of the Boltzmann weighed transmission probability is carried out using an 11-point Newton−Cotes quadrature formula. The Eckart potential is known to exhibit a narrower width than the actual tunneling path, which would result in an overestimation of the tunneling probability. However, this is compensated by the neglect of corner cutting in the zero-curvature approach.[12]

3. Results and Discussion

3.1. Hindered Rotation Partition Functions. The partition functions for the hindered internal rotation about the forming bond in the transition state and the breaking bond in the product radicals have been calculated according to the procedure described above. The maximal rotational barrier, the reduced moments of inertia, and the internal symmetry numbers determined from the optimized geometries are available in Table S1 of the Supporting Information. The asymmetric energy profiles for the internal rotations in reaction 2 and 3 can be found in Figures S1 and S2 of the Supporting Information.

The barrier for internal rotation in the transition state ranges from 0.4 to 4.4 kJ mol^{-1}, which is on the order of RT in the temperature range 50−500 K, and hence, both the harmonic oscillator and the free rotor approximation, which holds for barriers much higher and lower, respectively, than RT, are expected to yield an inaccurate partition function at the studied temperatures. The highest rotational barrier (4.4 kJ mol^{-1}) corresponds to the isopropyl addition to ethene (reaction 3) and is induced by the bulky nature of the added isopropyl radical. The lowest barrier, (0.4 kJ mol^{-1}) is found for the methyl addition to ethyne (reaction 7) in which the steric hindrance is minimal due to the sp hybridization of the attacked carbon atom.

For the internal rotations about the breaking bond in the product radicals, the rotational barriers range from 0 to 22.1 kJ mol^{-1}. No barrier is found for the isobutenyl radical of reaction 9, in which the methyl group rotates with respect to a resonance stabilized allylic fragment that is structurally similar to the methyl rotation in toluene, which is the prototypical free rotor. A barrier of 7.3 kJ mol^{-1} is found for reaction 7, the β-scission of a prop-1-en-1-yl radical, and the higher barriers are found for the β-scission of larger alkyl radicals in which ethyl and isopropyl radicals are split off (reactions 2 and 3). The other barriers range between 12 and 15 kJ mol^{-1}, the typical value for methyl rotors.

Figure 2a presents the ratios q_{HR}/q_{HO} as a function of temperature for the transition state of reaction 1 (methyl addition to ethene), reactions 2 and 3 (ethyl and isopropyl addition to ethene), reaction 7 (methyl addition to ethyne), and reaction 9 (methyl addition to allene). These include the reactions with the two largest and smallest ratios of the set.

In case conformers with higher energy are present, (e.g., in the transition states of the additions of ethyl and isopropyl radicals to ethene (reactions 2 and 3)) the HR partition function is larger than the HO partition function by a factor of approximately 3. For the transition states of reactions with threefold symmetric methyl internal rotors, the partition functions slightly decrease (i.e., the ratio q_{HR}/q_{HO} is generally smaller than unity). The largest reduction of q_{HR}/q_{HO} is observed for the methyl addition to ethyne and allene (reactions 7 and 9) due to the small rotational barriers. These findings are in agreement with the theoretical considerations illustrated in Figure 1; the ratio q_{HR}/q_{HO} is considerably larger for the asymmetrical model potential V_2. For all reactions, the ratio q_{HR}/q_{HO} decreases with increasing temperature.

The ratios of q_{HR}/q_{HO} for the product radicals (Figure 2b) show a similar pattern as that observed for the transition states: a significant increase in the partition function by a factor of 2−3 for reaction 2 and 3 due to the presence of higher energy conformers, and a ratio q_{HR}/q_{HO} close to unity for threefold symmetric internal rotors. The largest decrease, more than 1

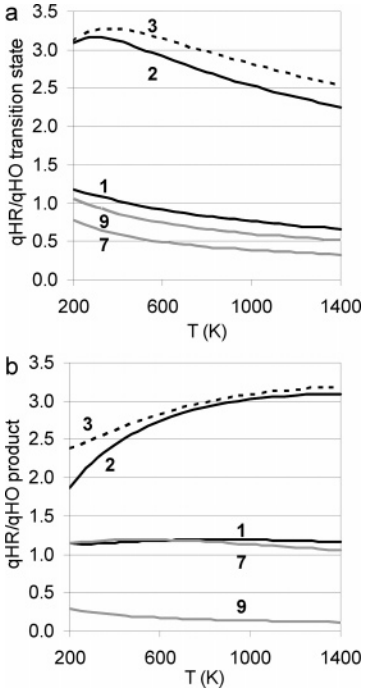

Figure 2. Ratios q_{HR}/q_{HO} vs T for (a) the transition state and (b) products of selected reactions.

order of magnitude for temperatures above 1000 K, is observed for the 2-methylprop-1-en-3-yl product of the addition of methyl to allene (reaction 9), which is a free rotor. The ratios of q_{HR}/q_{HO} for the product radicals of reactions 2 and 3 increase with increasing temperature. This reverse temperature dependence as compared to the partition functions in the transition state is due to the higher barrier to internal rotation.[25] The small reduction in the ratio q_{HR}/q_{HO} with increasing temperature for reaction 9 finds its origin in the very low rotational barrier. The temperature dependence for the other reactions is negligible.

3.2. Reaction Thermochemistry and Reaction Barrier. The reaction enthalpies for the reactions under study are calculated at the five studied levels of theory in both the HO and HR approach and are tabulated at 298 and 1000 K in Table S2 of the Supporting Information.

The differences in enthalpy between the HO and the HR approaches are smaller than 1 kJ mol^{-1} at 298 K and are smaller than 4 kJ mol^{-1} at 1000 K. The HR reaction enthalpies for reactions 1−6 increase of 2−8 kJ mol^{-1} from 298 to 1000 K, whereas for reaction 7, a decrease of 3−5 kJ mol^{-1} is observed. For reactions 8 and 9 no temperature influence on the HR reaction enthalpy is observed.

Figure 3 displays the HR reaction enthalpies for the different levels of theory. The CBS-QB3 and G3B3 reaction enthalpies are of similar magnitude, whereas the DFT methods yield lower values than CBS-QB3 and G3B3 for all reactions except for reactions 3, 6, and 9. The difference amounts to about 20 kJ mol^{-1} for reaction 7.

The calculated reaction enthalpies in the HR approximation are compared to reference values in Table 2 (298 K). Reference values for reaction enthalpies were calculated from NIST enthalpies of formation for the reactants and products,[26] from Benson group additivity (GA) when species were lacking in the NIST database,[9,40] or, for reaction 7 and 8 for which no Benson group additive values are present for the products, using semiempirical group additive values determined from bond additive corrected ab initio values.[41] The NIST reaction enthalpies were taken as the mean of the lowest and the highest reaction enthalpy if multiple enthalpies of formation were available.

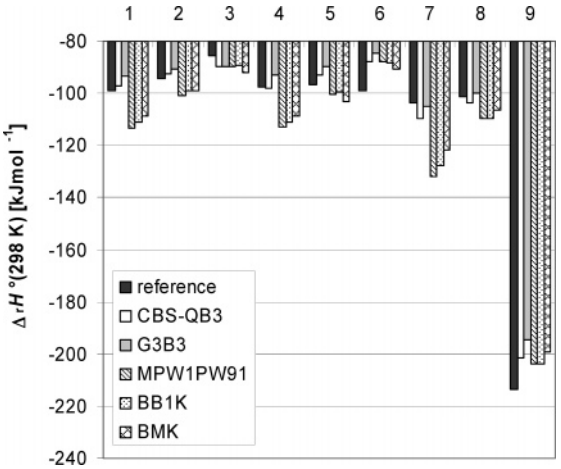

Figure 3. Calculated HR reaction enthalpies $\Delta_r H°(298\ K)$ and reference values (see text) for the set of nine reactions.

The CBS-QB3 method shows the best overall agreement to the reference values, closely followed by the G3B3 method. In general, the DFT methods underestimate the reaction enthalpies. The DFT methods provide better predictions than the CBS-QB3 and G3B3 methods only for reactions 6 and 9. For the latter two reactions there is a significant overestimation of 10−20 kJ mol^{-1} for all methods, raising doubt concerning the reliability of the reference value calculated from Benson group additivity values.

The mean absolute deviations (MAD) between calculated and reference reaction enthalpies show that CBS-QB3 performs best with a MAD of 4.8 kJ mol^{-1}. The G3B3 method has an accuracy of 6.8 kJ mol^{-1}. The MAD for the DFT methods is several kJ mol^{-1} higher, up to 11.3 kJ mol^{-1}.

Calculated reaction entropies ($\Delta_r S°$) for the addition reactions are tabulated in Table S3 in the Supporting Information (HO and HR approach, 298 and 1000 K).[42] At 298 K, the HR reaction entropies are 1.0−9.6 J mol^{-1} K^{-1} higher than the HO predictions, except for reaction 9, for which a decrease of 15.9 J mol^{-1} K^{-1} is observed due to the presence of a free rotor in the product radical; see also Figure 2. At 1000 K the differences remain similar, ranging between −0.4 and 10.5 J mol^{-1} K^{-1} for reactions 1−8 and −20.9 J mol^{-1} K^{-1} for reaction 9.

The temperature dependence of the reaction entropies varies more or less parallel to the temperature dependence of the reaction enthalpies, in line with Figure 1; from 298 to 1000 K, the reaction entropies increase for reactions 1−6 with 12.6 J mol^{-1} K^{-1} at the most; for reactions 7−9 there is a decrease up to 11.7 J mol^{-1} K^{-1}. The values for the reaction entropies all range between −160 and −120 J mol^{-1} K^{-1}.

The HR reaction entropies at 298 K are presented in Figure 4. The CBS-QB3, G3B3, MPW1PW91, and BB1K reaction entropies differ by less than 2.5 J mol^{-1} K^{-1}, except for reaction 9 where the BB1K reaction entropy deviates from the values obtained by the other methods by 5−7 J mol^{-1} K^{-1}. In general, the BMK method predicts lower reaction entropies that differ by up to more than 10 J mol^{-1} K^{-1} from those predicted by the other methods. For the two reactions for which NIST reference data[26] were available, the predicted reaction enthalpies are within 1.8 J mol^{-1} K^{-1} of experiment for reaction 1 and are within 2.6 J mol^{-1} K^{-1} of experiment for reaction 5, with exception for the BMK method which deviates by 11.7 J mol^{-1} K^{-1}.

TABLE 2: Calculated HR Standard Reaction Enthalpies $\Delta_r H°$(298K) Relative to Reference Reaction Enthalpies and MAD[a]

	$\Delta_r H°$ (ref) [kJ mol^{-1}]	source	$\Delta_r H°$(calc) − $\Delta_r H°$(ref) CBS-QB3	G3B3	MPW1PW91	BB1K	BMK
1	−98.9	NIST	1.7	5.2	−14.6	−12.3	−9.8
2	−94.2	Benson	1.6	3.4	−6.7	−4.9	−4.9
3	−85.7	Benson	−4.3	−4.1	−4.0	−3.7	−6.2
4	−97.8	NIST	−0.2	4.7	−15.2	−13.4	−10.8
5	−96.8	NIST	3.8	7.1	−3.8	−2.9	−6.3
6	−99.2	Benson	11.4	14.5	11.1	10.8	8.6
7	−103.8	Sabbe	−6.0	−1.4	−28.3	−23.9	−17.9
8	−101.2	Sabbe	−2.5	1.5	−8.6	−8.5	−5.3
9	−213.4	Benson	12.0	18.8	9.6	9.5	14.0
MAD			4.8	6.8	11.3	10.0	9.3

[a] The $\Delta_r H°$ reference values are calculated from NIST standard enthalpies of formation[26] or from Benson group additivity if species were lacking in the NIST database. Group additive values were taken from O'Neal and Benson[40] and Benson[9] or, if no GAVs were tabulated, from the GAVs of Sabbe.[41]

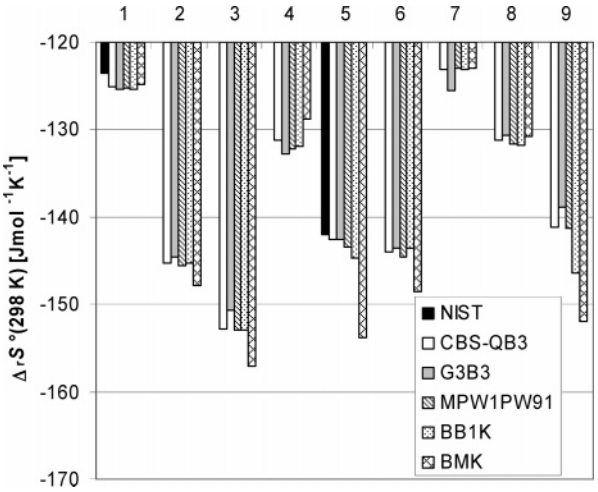

Figure 4. Calculated HR reaction entropies $\Delta_r S°$(298 K) and reference values taken from the NIST webbook[26] for the set of nine reactions.

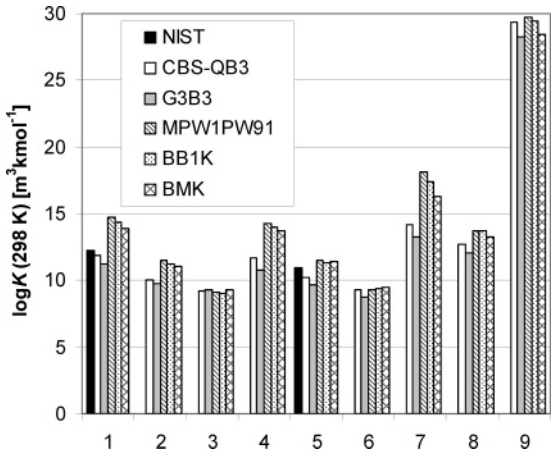

Figure 5. Calculated reaction equilibria in the HR approach at 298 K for the set of nine reactions.

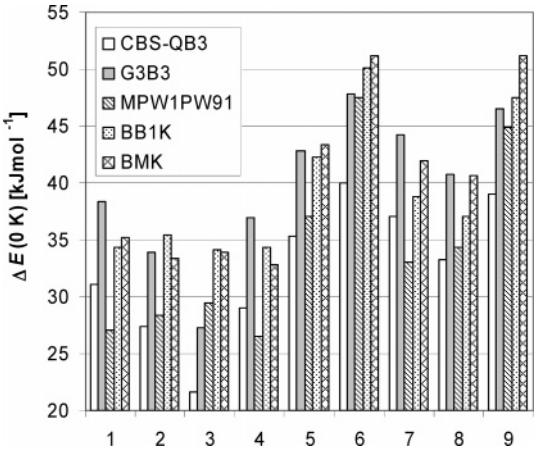

Figure 6. Calculated addition barriers at 0 K ΔE(0 K) for the set of nine reactions.

Because equilibrium coefficients are frequently used to ensure thermodynamic consistency in many applications, as is the case in reaction networks used for reactor simulations, the effect of the level of theory on the equilibrium coefficients has been considered. The differences between the HO and HR equilibrium coefficients derived from the calculated reaction thermochemistry are equal to the differences between the HO and HR product partition functions, as discussed in the previous section. The HR equilibrium coefficients at 298 K are presented in Figure 5. The addition equilibrium coefficients range between 10^9 and 10^{29} m^3 kmol^{-1}. The G3B3 HR equilibrium coefficients are systematically lower than the CBS-QB3 HR values; they are only slightly lower for most reactions but differ by up to 1 order of magnitude for reactions 4, 7, and 9. Most HR DFT equilibrium coefficients are much higher than CBS-QB3 and G3B3 values: 1 order of magnitude for reactions 2, 5, and 8, and up to 2−4 orders of magnitude for reactions 1, 4, and 7, mainly as a result of the lower reaction enthalpies than of the CBS-QB3 and G3B3 methods. Also, at 1000 K the DFT methods predict higher equilibrium coefficients than the other methods, but the differences are limited to about 1 order of magnitude because of the reduced dependency on the reaction enthalpy as compared to 298 K. In Figure 5 the calculated values are also compared to experimental equilibrium coefficients for the reactions for which NIST thermochemical values were available (reactions 1 and 5). For reaction 1, the CBS-QB3 and G3B3 predicted equilibrium coefficient is in good agreement with the experimental value, whereas the DFT methods overestimate the experimentally observed equilibrium coefficient by up to a factor of 300. For reaction 5, all methods provide a fairly good agreement to experiment.

Reaction barriers at 0 K are shown for the different computational methods in Figure 6 for addition and in Figure 7 for β-scission reactions. All transition state geometries are available in the Supporting Information. For additions, the reaction barriers range between 21.7 and 51.2 kJ mol^{-1} for all methods. The CBS-QB3 method predicts the lowest barriers, except for reactions 1, 4, and 7 for which the MPW1PW91 methods gives the lowest value. The G3B3 barriers are systematically 6−8 kJ mol^{-1} higher than those obtained with CBS-QB3; this systematic difference has been noted previously

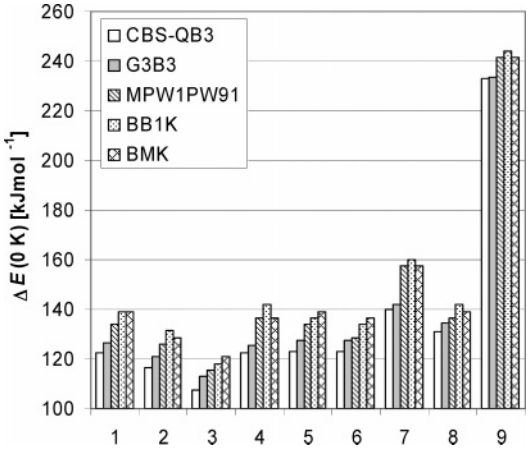

Figure 7. Calculated β-scission barriers at 0 K ΔE(0 K) for the set of nine reactions.

by other authors.[43] The BB1K and BMK barriers are similar to the G3B3 barriers; the BMK barrier exceeds the G3B3 barrier by about 5 kJ mol^{-1} for reactions 3 and 9 only. For the β-scission activation barriers, CBS-QB3 predicts the lowest barriers for all reactions. The G3B3 barriers are on average 4 kJ mol^{-1} higher than the CBS-QB3 barriers. The DFT methods predict barriers that are on average 6−10 kJ mol^{-1} higher than the G3B3 values. For reaction 7 the DFT methods find barriers that are 14−18 kJ mol^{-1} higher than the G3B3 barrier, which is related to the low reaction enthalpy calculated by the DFT methods for this reaction.

3.3. Rate Coefficients. Rate coefficients at 300 and 1000 K in the HO approach are reported in Table 3 for the five levels of theory selected in this study.

For addition reactions, the largest predictions are given by the CBS-QB3 (reactions 2, 3, 5, 6, and 9) or the MPW1PW91 DFT method (reactions 1, 4, 7, and 8). There is a striking resemblance between the rate coefficients of these two methods, even at different temperatures. The G3B3 rate coefficients are about a factor 10−20 smaller than the CBS-QB3 values at 300 K, but at 1000 K they are of comparable magnitude. The BB1K and BMK rate coefficients for addition are of the same magnitude as the G3B3 predictions at both temperatures.

For β-scissions too, CBS-QB3 provides the largest rate coefficients for all reactions. At 300 K, the G3B3 predictions are a lower by a factor of 2−10; at 1000 K they are of the same magnitude. However, the DFT functionals predict rate coefficients that are 1−3 orders of magnitude lower than the values calculated at the CBS-QB3 and G3B3 level of theory.

In Table 4 the mean factors $<\rho>$ describing the deviation between calculated and experimental rate coefficients are given. For the individual reactions, the ratios k_{calc}/k_{exp} are reported in Table S4 of the Supporting Information. For addition reactions, all methods perform rather well at 1000 K with all $<\rho>$ values lower than 6.1. At 300 K, the CBS-QB3 and MPW1PW91 methods perform well with $<\rho>$ factors of 2.1 and 9.6, respectively. The deviations are significantly larger for the G3B3, BB1K, and BMK methods, up to a $<\rho>$ value of 56 at 300 K. These methods predict higher barriers than the CBS-QB3 and MPW1PW91 methods, resulting in an underestimation of the experimentally observed addition rate coefficients. Remarkably, the DFT methods optimized for kinetics, the BB1K and the BMK methods, do not give better results than the MPW1PW91 functional.

The predicted rate coefficients for β-scissions are very accurate at 1000 K, with $<\rho>$ values ranging between 2.9, for the G3B3 method, and 3.9, for the CBS-QB3 and BB1K methods. At 300 K, the accuracy is even higher for the CBS-QB3 and G3B3 methods, with $<\rho>$ values of 3.2 and 1.9, respectively. At this temperature, the agreement of the DFT methods with experiment is rather disappointing; the $<\rho>$ values for these methods amount to 250, which is an even more pronounced deviation than for additions. This rather poor performance is caused by the severe underestimation of the β-scission rate coefficients, particularly for the β-scission of the 2-butyl radical into propene and methyl (reaction 4). The underestimation of the β-scission rate coefficients at 300 K is systematically more pronounced than for addition rate coefficients, implying that the studied DFT methods do not accurately predict the reaction equilibrium for these reactions. As already mentioned in section 3.2, the DFT methods predict equilibrium coefficients that are up to 4 orders of magnitude higher than the CBS-QB3 and G3B3 predictions at 300 K, which is mainly related to different predictions of the reaction enthalpy. The use of these DFT methods for the calculation of addition and β-scission rate coefficients is thus not recommended for low-temperature applications if an accurate description of thermodynamic equilibrium is of importance.

A comparison of the 5 studied levels of theory reveals that the CBS-QB3 and G3B3 methods are better suited for the calculation of rate coefficients and reaction equilibria for this set of hydrocarbon radical addition and β-scission reactions. For these two high accuracy compound methods, the effects of the hindered internal rotation and tunneling are assessed in what follows.

3.3.1. 1D-HR vs HO. The ratios of the rate coefficients k_{HR}/k_{HO} at 300, 600, and 1000 K are reported in Table 5. For addition reactions, the difference between the HO and HR rate coefficients coincides with the difference between the HO and HR partition functions for internal rotation in the transition state, as discussed in section 3.1. The ratios k_{HR}/k_{HO} range between 0.38 and 2.80 at 1000 K and between 0.67 and 3.29 at 300 K. In general, the HR treatment decreases the rate coefficient for the addition of methyl radicals ($k_{HR}/k_{HO} < 1$) whereas an increase is noted for the addition of larger radicals ($k_{HR}/k_{HO} > 1$) due to the presence of conformers with higher energy.

For β-scissions, the effect of the HR treatment on the rate coefficient results from the interplay between the ratios q_{HR}/q_{HO} of both the transition state and the product radical. The ratios k_{HR}/k_{HO} vary from 0.34 to 4.44 at 1000 K and from 0.58 to 4.00 at 300 K. For β-scissions, the rate coefficients decrease slightly except for the isobutenyl β-scission (reaction 9) due to the free rotor character of the methyl rotor in the product.

The ratios between calculated and experimental rate coefficients (k_{calc}/k_{exp}) are taken up in Table S5 for CBS-QB3 and Table S6 for G3B3 in the Supporting Information. For the CBS-QB3 method, all HR rate coefficients are within a factor of 8 from experiment, except for the data of the β-scission of 1-propyl (reaction 1) reported by Bencsura et al.[44] at 1000 K. The CBS-QB3 rate coefficients tend to overestimate experiment, but in general, this method succeeds in a fairly good reproduction of the rate coefficients.

For the G3B3 method, the ratios k_{calc}/k_{exp} range between 0.04 and 8.86. With the exception of the ethyl addition to ethene (reaction 2), the methyl addition to propene (reaction 5), and the methyl addition to ethyne at 300 K (reaction 7), the HR rate coefficients are within a factor of 8 for all reactions. At higher temperatures the deviation remains within a factor of 4, except for the data for the β-scission of 1-propyl (reaction 1) reported by Bencsura et al.[44] at 1000 K, as already noticed for

TABLE 3: Rate Coefficients for the Set of Nine Reactions[a]

	k_{HO} addition [m^3 $kmol^{-1}$ K^{-1}]					k_{HO} β-scission [s^{-1}]				
	CBS-QB3	G3B3	MPW1 PW91	BB1K	BMK	CBS-QB3	G3B3	MPW1 PW91	BB1K	BMK
					300 K					
1	2.6×10^3	1.4×10^2	8.1×10^3	9.1×10^2	5.1×10^2	5.1×10^{-9}	1.1×10^{-9}	2.3×10^{-11}	6.7×10^{-12}	9.5×10^{-12}
2	2.4×10^2	2.0×10^1	1.3×10^2	1.7×10^1	1.4×10^1	6.3×10^{-8}	9.7×10^{-9}	1.3×10^{-9}	3.1×10^{-10}	3.6×10^{-10}
3	1.4×10^3	1.7×10^2	8.1×10^1	1.6×10^1	9.1	3.0×10^{-6}	3.0×10^{-7}	2.0×10^{-7}	4.5×10^{-8}	1.5×10^{-8}
4	2.6×10^3	1.1×10^2	4.5×10^3	5.5×10^2	4.8×10^2	7.3×10^{-9}	2.6×10^{-9}	3.6×10^{-11}	8.3×10^{-12}	1.4×10^{-11}
5	1.1×10^2	5.3	3.7×10^1	6.8	4.8	8.8×10^{-9}	1.7×10^{-9}	1.6×10^{-10}	5.0×10^{-11}	2.6×10^{-11}
6	6.4	3.2×10^{-1}	3.0×10^{-1}	7.9×10^{-2}	4.1×10^{-2}	4.8×10^{-9}	7.9×10^{-10}	2.2×10^{-10}	4.4×10^{-11}	1.7×10^{-11}
7	1.9×10^3	9.5×10^1	8.2×10^3	8.0×10^2	2.9×10^2	1.9×10^{-11}	7.9×10^{-12}	1.1×10^{-14}	6.0×10^{-15}	2.4×10^{-14}
8	1.0×10^3	5.1×10^1	1.4×10^3	1.6×10^2	7.9×10^1	3.0×10^{-10}	6.7×10^{-11}	3.5×10^{-11}	4.3×10^{-12}	6.9×10^{-12}
9	1.6×10^2	9.7	2.1×10^1	2.8	1.2	3.0×10^{-28}	2.1×10^{-28}	1.5×10^{-29}	3.6×10^{-30}	1.8×10^{-29}
					1000 K					
1	5.5×10^7	2.2×10^7	7.8×10^7	4.0×10^7	3.3×10^7	2.1×10^7	1.4×10^7	4.4×10^6	3.1×10^6	3.1×10^6
2	2.2×10^6	1.1×10^6	1.9×10^6	1.1×10^6	9.6×10^5	3.4×10^7	2.0×10^7	1.1×10^7	7.3×10^6	9.0×10^6
3	2.9×10^6	1.9×10^6	1.3×10^6	9.0×10^5	4.4×10^5	1.2×10^8	6.0×10^7	5.9×10^7	4.2×10^7	2.5×10^7
4	4.0×10^7	1.5×10^7	4.7×10^7	2.6×10^7	3.2×10^7	3.2×10^7	2.6×10^7	7.1×10^6	4.6×10^6	5.0×10^6
5	8.4×10^6	3.5×10^6	6.2×10^6	3.7×10^6	3.4×10^6	3.9×10^7	2.4×10^7	1.3×10^7	1.0×10^7	2.8×10^7
6	1.9×10^6	8.7×10^5	8.4×10^5	5.3×10^5	3.4×10^5	1.8×10^7	1.1×10^7	8.1×10^6	4.4×10^6	4.0×10^6
7	1.9×10^8	5.9×10^7	3.1×10^8	1.8×10^8	9.3×10^7	2.6×10^7	2.0×10^7	2.9×10^6	2.9×10^6	2.9×10^6
8	4.3×10^7	1.7×10^7	4.7×10^7	2.6×10^7	2.1×10^7	2.2×10^7	1.3×10^7	1.2×10^7	7.2×10^6	7.2×10^6
9	4.4×10^7	2.3×10^7	2.0×10^7	1.0×10^7	6.8×10^6	7.2×10^1	6.3×10^1	2.5×10^1	2.5×10^1	5.2×10^1

[a] Calculated in the HO approximation at the five studied levels of theory (300 and 1000 K).

TABLE 4: Mean Deviation Factor $<\rho>$, According to Expression 5, for the Rate Coefficients in the Harmonic Oscillator Approximation of the Set of Nine Reactions

	$<\rho>$ addition					$<\rho>$ β-scission				
T (K)	CBS-QB3	G3B3	MPW1 PW91	BB1K	BMK	CBS-QB3	G3B3	MPW1 PW91	BB1K	BMK
300	2.1	16.0	9.6	33.9	56.0	3.2	1.9	50.3	205.4	166.4
600	4.2	3.0	6.9	4.8	5.1	2.8	2.2	5.3	10.3	8.7
1000	5.2	3.3	6.1	4.3	4.3	3.9	2.9	3.5	3.9	3.2
mean	3.8	7.4	7.6	14.4	21.8	3.3	2.3	19.7	73.2	59.4

TABLE 5: Ratios k_{HR}/k_{HO} between Rate Coefficients in the Hindered Rotor and Harmonic Oscillator Approach

	k_{HR}/k_{HO} addition			k_{HR}/k_{HO} β-scission		
	300 K	600 K	1000 K	300 K	600 K	1000 K
1	1.09	0.91	0.75	0.96	0.79	0.67
2	3.13	2.91	2.48	1.44	1.06	0.82
3	3.29	3.09	2.80	1.33	1.14	0.92
4	1.10	0.94	0.76	0.99	0.78	0.63
5	1.14	1.04	0.91	1.05	0.91	0.77
6	1.18	1.08	0.95	1.06	0.93	0.78
7	0.67	0.49	0.38	0.58	0.41	0.34
8	1.15	0.93	0.77	1.00	0.81	0.68
9	0.95	0.75	0.60	4.00	4.17	4.44

the HR CBS-QB3 method. The rate coefficient reported by Benscura et al. is rather low as compared to the other expertimental values. In general, the G3B3 method tends to underestimate the experimentally observed rate coefficients, particularly at 300 K, as illustrated in Figures 8−10 that show the Arrhenius plots for reactions 1, 3, and 7.

The G3B3 rate coefficients are lower than the CBS-QB3 rate coefficients due to the 6−8 kJ mol^{-1} higher barriers at 0 K, as discussed in section 3.1. The activation entropies, which differ for these two methods by, at most, 2.3 J mol^{-1} K^{-1} at 300 K, have only a secondary effect on the differences between the CBS-QB3 and G3B3 rate coefficients.

Figures 8−10 illustrate the overall improvement introduced by the hindered rotation approach in reproducing the experimental rate coefficients. At lower temperatures there is only a minor influence, except for reactions 2 and 3 in which higher energy conformers are present. To quantify the deviation between calculated and experimental values, the $\langle\rho\rangle$ value is calculated (see Table 6), confirming the better performance of the hindered rotor for both methods and at all studied temperatures, except for β-scissions at 300 K, for which no significant influence is found. Overall, the HR approach improves the $<\rho>$ value by about 25% for both computational methods. These findings agree with results reported by Gómez-Balderas et al.,[43] who compare the free rotor, hindered rotor, and harmonic oscillator approaches for a set of four methyl additions at 298 K.

3.3.2. Tunneling. The corrections for tunneling calculated using the Wigner, Skodje and Truhlar, and Eckart methods are tabulated in Table S7 of the Supporting Information. The values of the imaginary frequencies are mainly correlated with the electronic barrier height and range between 444 and 560 cm^{-1}

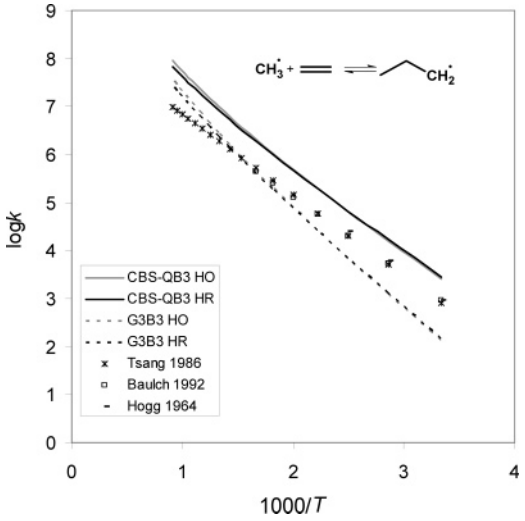

Figure 8. Arrhenius plot for the reaction $CH_3^\bullet + C_2H_4 \rightarrow C_3H_7^\bullet$: CBS-QB3 and G3B3 rate coefficients in the HO and HR approach and comparison to experimental reference (m^3 $kmol^{-1}$ s^{-1}).

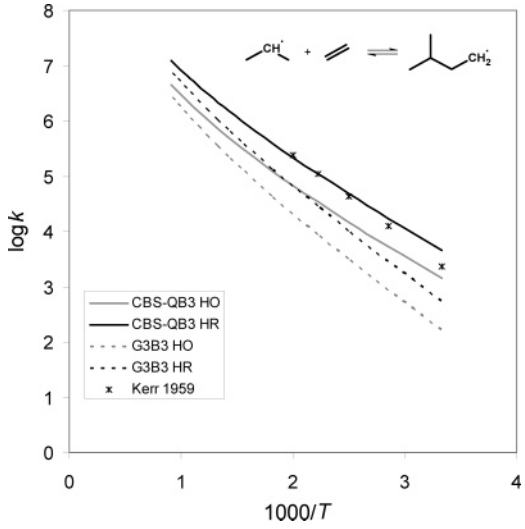

Figure 9. Arrhenius plot for the reaction *iso*-$C_3H_7^\bullet + C_2H_4 \rightarrow C_5H_{11}^\bullet$: CBS-QB3 and G3B3 rate coefficients in the HO and HR approach and comparison to experimental reference (m^3 $kmol^{-1}$ s^{-1}).

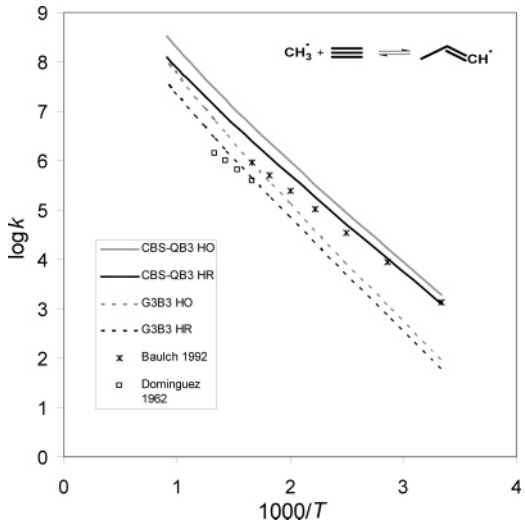

Figure 10. Arrhenius plot for the reaction $CH_3^\bullet + C_2H_2 \rightarrow C_3H_5^\bullet$: CBS-QB3 and G3B3 rate coefficients in the HO and HR approach and comparison to experimental reference (m^3 $kmol^{-1}$ s^{-1}).

for CBS-QB3 and between 465 and 577 cm^{-1}, resulting in rather small tunneling corrections. At temperatures above 600 K, tunneling corrections for all three methods increase the CBS-QB3 and G3B3 HR-rate coefficient by 9% at most. At 300 K, the tunneling corrections amount to a 40% increase, with the tunneling coefficients for the G3B3 method slightly higher than for the CBS-QB3 method due to the somewhat higher electronic barriers (see section 3.1) and imaginary frequencies. The tunneling correction methods of Skodje and Truhlar and Eckhart yield tunneling coefficients that are higher than for the Wigner method; for the G3B3 rate coefficients the tunneling correction amounts, on average, to 30% (Skodje and Truhlar and Eckart) as compared to 25% for the Wigner correction.

Because the CBS-QB3 HR-rate coefficients generally exceed the experimental rate coefficient over the entire temperature range, inclusion of tunneling does not improve the agreement with experiment, especially not in the lower temperature range. The main $<\rho>$ value for addition reactions (see Table 6) increases from 3.1 to 3.2−3.3 upon inclusion of tunneling corrections. In contrast, the G3B3 method generally underestimates the experimental rates, particularly in the lower temperature range. Therefore, for G3B3, inclusion of tunneling corrections improves the agreement with experiment for the majority of the reactions. Overall, the main $<\rho>$ value (see Table 6) decreases by 20% from 5.3 to 4.4−4.5 upon inclusion of tunneling corrections. The methods of Skodje and Truhlar and Eckart provide a slightly better agreement to experimental rate coefficients. For β-scissions the results are similar: an increase in the $<\rho>$ value from 2.8 to 3.0−3.1 for the CBS-QB3 method and a small decrease from 2.0 to 1.9 for G3B3. All three tunneling approximations give the same result for β-scissions.

A comparison of the $<\rho>$ values for the CBS-QB3 and the G3B3 methods in Table 6 shows that for addition reactions the CBS-QB3 HR rate coefficients provide better agreement with experiment than the G3B3 HR rate coefficients using Skodje and Truhlar (HR+ST) or Eckhart tunneling contributions (HR+E). In contrast, for β-scission reactions, the G3B3 HR+ST and HR+E rate coefficients corrected for tunneling provide better agreement with experiment than the CBS-QB3 HR rate coefficients.

As suggested by IUPAC, a measure for the uncertainty on rate coefficients obtained with theoretical methods can be determined as twice the average deviation in a test set.[45] According to this procedure, an uncertainty factor on the calculated rate coefficients can be obtained as twice the $<\rho>$ value. For both the CBS-QB3 HR and the G3B3 HR+E methods, the $<\rho>$ values averaged over addition and β-scission reactions and all temperatures amounts to 3, the uncertainty factor on the calculated rate coefficients amounts to 6.

3.4. HR Arrhenius Parameters. In this section, the effect of hindered internal rotation on the activation energy is discussed first, followed by a discussion of the effect on the pre-exponential factor. Last, the influence of tunneling will be discussed. The Arrhenius parameters for the best performing methods (i.e., CBS-QB3 HR and G3B3 HR+E) are reported in Table 7. The Arrhenius parameters for the HO, HR, and HR+E approaches are available in Table S8 of the Supporting Information.

For activation energies, the hindered rotor treatment for all addition and β-scission reactions results in a systematic decrease as compared to the HO approach, except for the β-scission of reaction 9 in which a free rotor in the reactant radical is present. This effect of the HR approach on Arrhenius parameters is in accordance to the theoretical considerations presented in Figure 1. The effect is most pronounced at higher temperaturesp; at 1000 K the average decrease in activation energy is 3.1 kJ mol^{-1} for additions and 2.6 kJ mol^{-1} for β-scissions. At 300 K, the activation energies vary by less than 1 kJ mol^{-1} because at lower temperatures the HO approach provides a reasonable approximation of a hindered rotor. The differences between HO and HR Arrhenius parameters are illustrated in Figure 11 for reaction 1 and the two highest and lowest extrema (i.e., reactions 2, 3, 7, and 9). For addition reactions, the activation energy varies linearly with temperature, and reaction 7 almost exhibits the free rotor behavior of $-RT/2$. For β-scissions, Figure 11 illustrates that the variation in activation energy is less systematic and tends to be smaller in magnitude than for additions.

The impact of the HR on the pre-exponential factor is less systematic than the effect on activation energies; at 1000 K the variations on the pre-exponential factor $\Delta(\log A)$ range between −0.62 and 0.33 for additions and between −0.60 and 0.68 for β-scissions. These values correspond to a maximal change of a factor of ∼4 on the pre-exponential factor A. An increase of A is generally observed for reactions showing higher energy conformers in the internal rotational potential, such as the

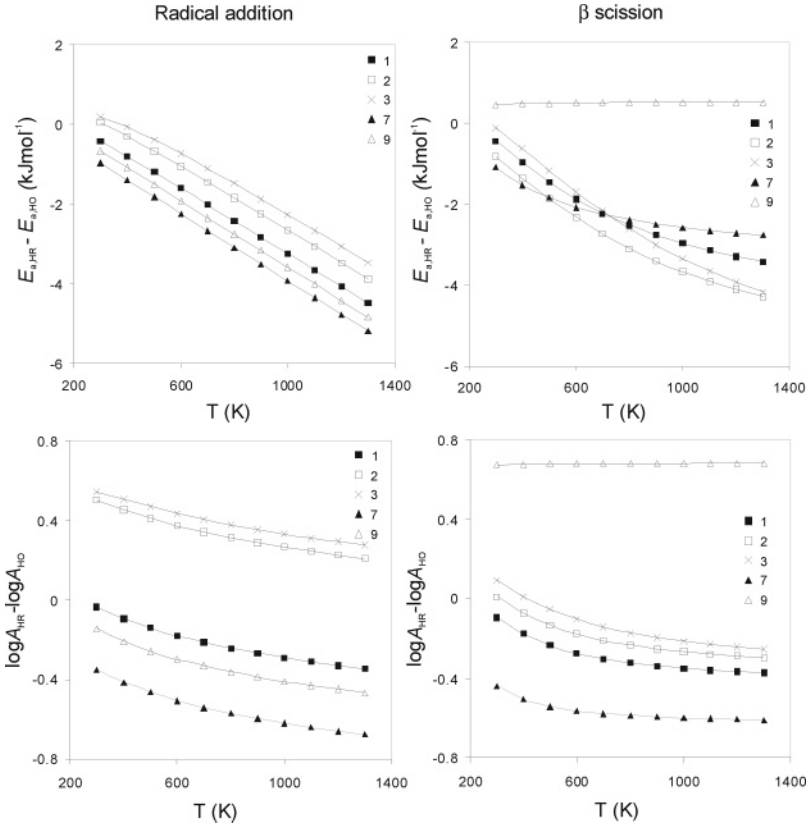

Figure 11. Difference between HO and HR Arrhenius parameters vs T for reactions 1−3, 7, and 9 (left: additions; right: β-scissions).

TABLE 6: Mean Deviation Factor $<\rho>$ According to Expression 5

	$<\rho>$ addition					$<\rho>$ β scission				
T (K)	k_{HO}	k_{HR}	k_{HR+W}	k_{HR+ST}	k_{HR+E}	k_{HO}	k_{HR}	k_{HR+W}	k_{HR+ST}	k_{HR+E}
					CBS-QB3					
300	2.1	2.1	2.4	2.5	2.5	3.2	3.3	4.0	4.1	4.1
600	4.2	3.2	3.4	3.4	3.4	2.8	2.5	2.6	2.6	2.6
1000	5.2	3.9	4.0	4.0	4.0	3.9	2.6	2.6	2.6	2.6
mean	3.8	3.1	3.2	3.3	3.3	3.3	2.8	3.0	3.1	3.1
					G3B3					
300	16.0	11.6	9.3	8.9	8.9	1.9	1.9	1.6	1.6	1.6
600	3.0	2.2	2.1	2.1	2.1	2.2	2.1	2.1	2.1	2.1
1000	3.3	2.3	2.3	2.3	2.3	2.9	1.9	1.9	1.9	1.9
mean	7.4	5.3	4.5	4.4	4.4	2.3	2.0	1.9	1.9	1.9

TABLE 7: Calculated Arrhenius Parameters for the CBS-QB3 HR and the G3B3 HR+E Methods[a]

	CBS-QB3 HR								G3B3 HR+E							
	300 K				1000 K				300 K				1000 K			
	radical addition		β-scission		radical addition		β-scission		radical addition		β-scission		radical addition		β-scission	
	log A	E_a	log A	E_a	log A	E_a	log A	E_a	log A	E_a	log A	E_a	log A	E_a	logA	E_a
1	8.785	30.5	13.485	125.1	9.871	43.1	13.848	128.5	8.650	36.5	13.365	127.6	9.847	50.0	13.841	131.9
2	7.737	27.8	13.511	118.0	8.890	41.0	13.704	119.8	7.669	33.0	13.405	121.5	8.941	47.2	13.711	124.1
3	7.573	22.3	13.743	109.9	8.814	36.3	13.800	110.2	7.559	26.9	13.620	114.4	8.932	42.0	13.786	115.6
4	8.587	29.4	13.614	124.9	9.677	42.0	14.047	129.0	8.460	35.9	13.560	126.5	9.661	49.4	14.117	131.7
5	8.278	35.4	13.894	125.9	9.415	48.4	14.197	128.6	8.139	41.4	13.759	128.6	9.416	55.6	14.197	132.4
6	7.895	40.2	13.593	125.6	9.054	53.4	13.815	127.5	7.784	46.2	13.457	128.6	9.106	60.8	13.828	131.7
7	9.464	36.5	14.034	143.5	10.277	46.1	14.859	151.4	9.156	41.3	13.844	143.7	10.071	51.7	14.838	152.9
8	8.850	33.1	13.860	134.2	9.888	45.2	14.486	140.2	8.710	39.2	13.686	136.3	9.877	52.3	14.421	143.1
9	9.026	39.3	14.536	238.0	10.14	52.1	15.336	245.5	8.939	44.8	14.326	236.7	10.252	59.3	15.298	245.6

[a] 300 and 1000 K. E_a is measured in units of kJ mol^{-1}, and log A is measured in units of m^3 kmol^{-1} s^{-1} for additions and s^{-1} for β-scissions.

additions of ethyl and isopropyl radicals (reactions 2 and 3), see Figure 11. At 300 K, the influence of HR becomes minor, except for reactions 2 and 3, in which log A increases due to the inclusion of higher energy conformers, and for reactions 7 and 9, which have a free rotor in, respectively, the transition state and the resulting reactant radical.

The effect of tunneling on the G3B3 Arrhenius parameters is a small decrease of 1.3−2.1 kJ mol^{-1} on activation energies

and an average decrease of 0.15 of the pre-exponential factor at 300 K (See Table S9 in Supporting Information). At 1000 K, the average changes are reduced to -0.4 and -0.01 kJ mol^{-1}, respectively.

Arrhenius parameters for the set of reactions are reported in Table 7 for the best performing methods (i.e., CBS-QB3 HR and G3B3 HR+E). For additions, the G3B3 HR+E activation energies are systematically 5−7 kJ mol^{-1} higher than the CBS-QB3 HR. For β-scissions, the G3B3 HR values are, in general, 2−4 kJ mol^{-1} higher. The G3B3 HR+E pre-exponential factors are similar to the CBS-QB3 HR pre-exponential factors at 1000K. At 300 K the G3B3 HR+E pre-exponential factor (log *A*) are systematically lower, on average, by 0.13 kJ mol^{-1} for additions and 0.14 kJ mol^{-1} for β-scissions, which is caused by the inclusion of tunneling in the G3B3 HR+E pre-exponential factors and not by the G3B3 method itself. In the absence of tunneling contributions and also at 300 K, the G3B3 pre-exponential factors are very similar to the CBS-QB3 HR values.

4. Conclusions

For a set of nine reactions, ab initio rate coefficients were calculated with the compound methods CBS-QB3 and G3B3 and three DFT functionals, MPW1PW91, BB1K, and BMK. Five different computational approaches of hindered rotation and tunneling were compared: the harmonic oscillator approach, the hindered rotor approach, and the hindered rotor approach combined with three different tunneling corrections (i.e., the Wigner, the Skodje and Truhlar, and the Eckart methods).

All three considered DFT methods are computationally much less demanding than the high-level compound methods, but they provide rate coefficient predictions that do not allow an accurate description of the experimentally observed equilibrium for this set of reactions, particularly not at lower temperatures. The DFT methods predict reaction enthalpies that are generally lower by 5−15 kJ mol^{-1} than the CBS-QB3 and G3B3 values and tend to underestimate the experimental reference values.

For the studied hydrocarbon radical addition and β-scission reactions, corrections for hindered internal rotation about the forming/breaking bond in transition state and product radical significantly improve the agreement with experimental values, particularly at higher temperatures. The improvement is most pronounced for addition reactions.

CBS-QB3 tends to overestimate the reference rate coefficients, whereas the G3B3 method underestimates the latter. Therefore, the inclusion of tunneling only improves G3B3 rate coefficients. The best agreement with experimental data for this set of reactions is obtained by the CBS-QB3 method including corrections for hindered internal rotation (CBS-QB3 HR) and by the G3B3 method including corrections for hindered internal rotation and Skodje and Truhlar or Eckart tunneling corrections (G3B3 HR+ST or G3B3 HR+E). Both methods have a reasonable average factor of deviation with experimental rate coefficients of about 3.

Acknowledgment. Financial support from the Fund for Scientific Research-Flanders (F.W.O.-Vlaanderen) is acknowledged. M.K.S. holds a Ph.D. grant of the Institute for the Promotion of Innovation through Science and Technology in Flanders (IWT-Vlaanderen).

Notation

A =	pre-exponential factor (m^3 kmol^{-1} s^{-1} or s^{-1})
E_a =	activation energy (J mol^{-1})
ΔE_0 =	electronic activation barrier (excluding ZPVE) (J mol^{-1})
ΔE(0 K) =	activation barrier at 0 K (including ZPVE) (J mol^{-1})
I_{red} =	reduced moment of inertia for internal rotation (kg m^2)
k_∞ =	high-pressure rate coefficient (m^3 kmol^{-1}s^{-1} or s^{-1})
n_{opt} =	number of optical isomers
q =	molecular partition function
V_i =	cosine Fourier expansion coefficient for $V(\varphi)$ (J mol^{-1})
V_i' =	sine Fourier expansion coeffient for $V(\varphi)$ (J mol^{-1})
$V(\varphi)$ =	potential energy profile for internal rotation (J mol^{-1})
ZPVE =	zero point vibrational energy (J mol^{-1})
κ =	tunneling coefficient
σ =	symmetry number

Acronyms

1D-HR =	one-dimensional uncoupled hindered rotation treatment of internal rotor
HO =	harmonic oscillator
HR =	hindered rotation treatment of rotation about forming/breaking bond in transition state and product radical
HR+E =	HR+Eckart tunneling correction
HR+ST =	HR+Skodje and Truhlar tunneling corrections
HR+W =	HR+Wigner tunneling correction
PES =	potential energy surface.

Supporting Information Available: Part one: Discussion of experimental values from the NIST chemical kinetics web site. Parameters used for the calculation of the hindered rotor partition functions, Table S1. Calculated reaction enthalpies and entropies at the five studied levels of theory using the HO and HR approaches (298 and 1000 K), Tables S2 and S3, respectively. Ratios between calculated and experimental rate coefficients for the five studied levels of theory in the HO approach, Table S4. Ratios between calculated and experimental rate coefficients for the CBS-QB3 and G3B3 methods for all approaches HO, HR, HR+W, HR+ST, and HR+E (300, 600, and 1000 K), Tables S5 and S6, respectively. Electronic barriers, imaginary frequencies, and tunneling coefficients for the three studied tunneling methods, Table S7. Arrhenius parameters for the CBS-QB3 and G3B3 method for the HO, HR, and HR+E approaches (300, 600, and 1000 K), Tables S8 and S9, respectively. Part two: Transition state geometries for the five studied levels of theory. This material is available free of charge via the Internet at http://pubs.acs.org.

References and Notes

(1) Clymans, P. J.; Froment, G. F. *Comp. Chem. Eng.* **1984**, *8*, 137−142.

(2) Hillewaert, L. P.; Dierickx, J. L.; Froment, G. F. *AIChE J.* **1988**, *34*, 17−24.

(3) Ranzi, E.; Dente, M.; Plerucci, S.; Biardi, G. *Ind. Eng. Chem. Fund.* **1983**, *22*, 132−139.

(4) Zador, J.; Zsely, I. G.; Turanyi, T.; Ratto, M.; Tarantola, S.; Saltelli, A. *J. Phys. Chem. A* **2005**, *109*, 9795−9807.

(5) Susnow, R. G.; Dean, A. M.; Green, W. H.; Peczak, P.; Broadbelt, L. J. *J. Phys. Chem. A* **1997**, *101*, 3731−3740.

(6) Green, W. H.; Barton, P. I.; Bhattacharjee, B.; Matheu, D. M.; Schwer, D. A.; Song, J.; Sumathi, R.; Carstensen, H. H.; Dean, A. M.; Grenda, J. M. *Ind. Eng. Chem. Res.* **2001**, *40*, 5362−5370.

(7) Evans, M. G.; Polanyi, M. *Proc. Roy. Soc. A* **1936**, *154*, 1333−1360.

(8) Evans, M. G.; Polanyi, M. *Trans. Faraday Soc.* **1938**, *1938*, 11−29.

(9) Benson, S. W. *Thermochemical Kinetics*, 1st ed.; John Wiley & Sons Ltd.: New York, 1968.

(10) Willems, P. A.; Froment, G. F. *Ind. Eng. Chem. Res.* **1988**, *27*, 1959−1966.
(11) Willems, P. A.; Froment, G. F. *Ind. Eng. Chem. Res.* **1988**, *27*, 1966−1971.
(12) Truong, T. N.; Duncan, W. T.; Tirtowidjojo, M. *Phys. Chem. Chem. Phys.* **1999**, *1*, 1061−1065.
(13) Sumathi, R.; Carstensen, H. H.; Green, W. H. *J. Phys. Chem. A* **2001**, *105*, 8969−8984.
(14) Zhang, S. W.; Truong, T. N. *J. Phys. Chem. A* **2003**, *107* (8), 1138−1147.
(15) Saeys, M.; Reyniers, M. F.; Marin, G. B.; Van Speybroeck, V.; Waroquier, M. *AIChE J.* **2004**, *50*, 426−444.
(16) Montgomery, J. A.; Frisch, M. J.; Ochterski, J. W.; Petersson, G. A. *J. Chem. Phys.* **1999**, *110*, 2822−2827.
(17) Baboul, A. G.; Curtiss, L. A.; Redfern, P. C.; Raghavachari, K. *J. Chem. Phys.* **1999**, *110*, 7650−7657.
(18) Adamo, C.; Barone, V. *J. Chem. Phys.* **1998**, *108*, 664−675.
(19) Zhao, Y.; Lynch, B. J.; Truhlar, D. G. *J. Phys. Chem. A* **2004**, *108*, 2715−2719.
(20) Boese, A. D.; Martin, J. M. L. *J. Chem. Phys.* **2004**, *121*, 3405−3416.
(21) Van Speybroeck, V.; Van Neck, D.; Waroquier, M.; Wauters, S.; Saeys, M.; Marin, G. B. *J. Phys. Chem. A* **2000**, *104*, 10939−10950.
(22) Heuts, J. P. A.; Gilbert, R. G.; Radom, L. *Macromolecules* **1995**, *28*, 8771−8781.
(23) Van Speybroeck, V.; Vansteenkiste, P.; Van Neck, D.; Waroquier, M. *Chem. Phys. Lett.* **2005**, *402*, 479−484.
(24) Vansteenkiste, P.; Van Speybroeck, V.; Marin, G. B.; Waroquier, M. *J. Phys. Chem. A* **2003**, *107*, 3139−3145.
(25) Vansteenkiste, P.; Van Neck, D.; Van Speybroeck, V.; Waroquier, M. *J. Chem. Phys.* **2006**, *124*, Art. No. 044314.
(26) Afeefy, H. Y.; Liebman, J. F.; Stein, S. E. Neutral Thermochemical Data. In *NIST Chemistry WebBook, NIST Standard Reference Database Number 69*, Lindstrom, P. J., Mallard, W. G., Eds.; National Institute of Standards and Technology: Gaithersburg, Maryland, 2005.
(27) *Gaussian 03, rev. B.03*, Gaussian, Inc.: Wallingford Connecticut, 2004.
(28) Saeys, M.; Reyniers, M. F.; Marin, G. B.; Van Speybroeck, V.; Waroquier, M. *J. Phys. Chem. A* **2003**, *107*, 9147−9159.
(29) Montgomery, J. A.; Frisch, M. J.; Ochterski, J. W.; Petersson, G. A. *J. Chem. Phys.* **2000**, *112*, 6532−6542.
(30) Andersson, M. P.; Uvdal, P. *J. Phys. Chem. A* **2005**, *109*, 2937−2941.
(31) East, A. L. L.; Radom, L. *J. Chem. Phys.* **1997**, *106*, 6655−6674.
(32) Van Cauter, K.; Van Speybroeck, V.; Vansteenkiste, P.; Reyniers, M. F.; Waroquier, M. *Chem. Phys. Chem.* **2006**, *7*, 131−140.
(33) Masgrau, L.; Gonzalez-Lafont, K.; Lluch, J. M. *J. Comput. Chem.* **2003**, *24*, 701−706.
(34) McQuarrie, D. A.; Simon, J. D. *Molecular Thermodynamics;* University Science Books: Sausalito, 1999.
(35) Hirschfelder, J. O.; Wigner, E. *J. Chem. Phys.* **1939**, *7*, 616.
(36) Skodje, R. T.; Truhlar, D. G.; Garrett, B. C. *J. Phys. Chem.* **1981**, *85*, 3019−3023.
(37) Eckart, C. *Phys. Rev.* **1930**, *35*, 1303−1309.
(38) Cramer, C. J. *Essentials of Computational Chemistry: Theories and Models*; 2nd ed.; Wiley: Chichester, 2005.
(39) Coote, M. L.; Collins, M. A.; Radom, L. *Mol. Phys.* **2003**, *101*, 1329−1338.
(40) O'Neal, H. E.; Benson, S. W. Thermochemistry of free radicals. In *Free Radicals*, Kochi, J. K., Ed.; Wiley: New York, 1973; pp 275−359.
(41) Sabbe, M. K.; Saeys, M.; Reyniers, M. F.; Marin, G. B.; Van Speybroeck, V.; Waroquier, M. *J. Phys. Chem. A* **2005**, *109*, 7466−7480.
(42) For the calculation of the partition function of the 2-propyl radical of reaction 3, the external symmetry number of 2 was applied manually because all ab initio methods determined the species as having only *Cs* symmetry.
(43) Gomez-Balderas, R.; Coote, M. L.; Henry, D. J.; Radom, L. *J. Phys. Chem. A* **2004**, *108*, 2874−2883.
(44) Bencsura, A.; Knyazev, V. D.; Xing, S.-B.; Slagle, I. R.; Gutman, D. *Symp. Int. Combust. Proc.* **1992**, *24*, 629−635.
(45) Berces, T. IUPAC Critical evaluation of thermochemical properties of selected radicals. Part 1. *https://cmcs.ca.sandia.gov/cmcs/portal*, 2003.